Available online at www.sciencedirect.com

ScienceDirect

Proceedings of the Combustion Institute 38 (2021) 881–889

Proceedings of the Combustion Institute

www.elsevier.com/locate/proci

A single pulse shock tube study of pentene isomer pyrolysis

Shashank S. Nagaraja [a,*], Jennifer Power [a], Goutham Kukkadapu [b,*], Shijun Dong [a], Scott W. Wagnon [b], William J. Pitz [b], Henry J. Curran [a]

[a] *Combustion Chemistry Centre, School of Chemistry, Ryan Institute, MaREI, National University of Ireland Galway, Ireland*

[b] *Lawrence Livermore National Laboratory, Livermore, CA 94551, USA*

Received 7 November 2019; accepted 28 June 2020
Available online 2 August 2020

Abstract

A single-pulse shock tube study of the four pentene isomers is carried out at 2 ± 0.16 bar and 900–1600 K. C_1 to C_6 species profiles were recorded using gas chromatography mass spectrometry analyses. The species are identified using mass spectrometry and quantified by flame ionization detection. High-pressure limiting and pressure-dependent rate constants for 2M1B, 2M2B and 3M1B + $\dot{H}$ were calculated using RRKM theory with a Master Equation (ME) analysis using the Master Equation System Solver, MESS. A mechanism was formulated based on rate rules and theoretical calculations. Comparisons between experimental results and model simulations are provided for all of the five pentene isomers investigated with satisfactory agreement. Furthermore, an insight is provided into the influence of molecular structure on the reactivity of pyrolysis chemistry. Interestingly, it is found that the HACA mechanism is much less prominent for benzene formation compared to the role of cyclopentadienyl radical recombination with methyl radicals and also the recombination of propargyl radicals.

Keywords: Single pulse shock tube; Gas chromatography mass spectrometry; Chemical kinetics; Pentene isomers; Benzene formation

1. Introduction

Alkenes are one of the major components of commercial fuels and understanding their consumption reactions is important in producing more accurate predictions of their pyrolysis and oxidation in combustors. The oxidation of alkenes has been widely studied due to their importance as intermediates during ignition of alkanes and they are also known to impart higher octane sensitivity (RON – MON) in commercial fuels [1]. In addition, olefins are precursors to allene, propyne and isomers of butadiene which are known to be

* Corresponding authors.
E-mail addresses: s.sakleshpurnagaraja1@nuigalway.ie (S.S. Nagaraja), kukkadapu1@llnl.gov (G. Kukkadapu).

https://doi.org/10.1016/j.proci.2020.06.069

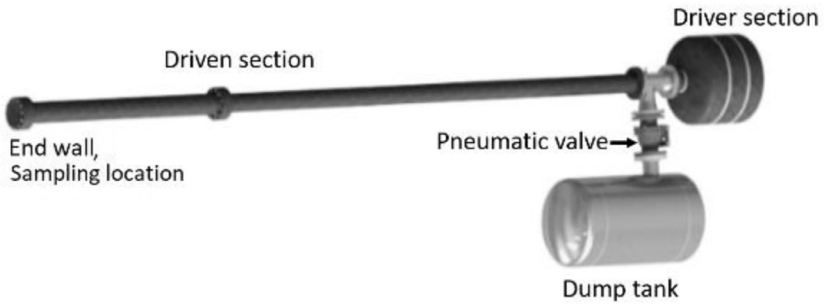

Fig. 1. Schematic of the NUIG SPST.

important intermediates in the formation of benzene and polycyclic aromatic hydrocarbons (PAHs) [2,3]. Furthermore, recent studies have shown the importance of C_5 species i.e. pentadiene isomers and cyclopentadiene [4–6] in the formation of benzene and naphthalene, among others. This explains our interest in studying the pyrolysis of C_5 species.

Although there have been a few studies related to the oxidation of 1-pentene [7–10], pyrolysis studies providing species profiles for reactants, intermediates and products are scarce. Tsang [11] performed a few 1-pentene pyrolysis experiments at 1000–1200 K during his study of cyclopentane but no further pyrolysis experiments are available. Manion and Awan [12] performed experiments of 2-pentene pyrolysis with hydrogen radical precursors in their study of the decomposition of pentyl radicals. Westbrook et al. [13] carried out an experimental and modeling study on 2-methyl-2-butene (2M2B) in a shock tube and in a jet-stirred reactor. Ruwe et al. [14] studied the consumption and hydrocarbon growth processes in a 2M2B flame. Furthermore, in a different study, Ruwe et al. [15] studied and demonstrated the effect of molecular structure on sooting tendencies of *n*-pentane, 1-pentene and 2M2B. From our literature review it is clear that the pyrolysis of the C_5 olefins is not well studied and structural effects influencing the formation of aromatics are not clearly understood. Therefore we have studied the pyrolysis of the five pentene isomers in a single pulse shock-tube and carried out gas chromatography/mass spectrometry (GC–MS) analyses. Several important C_1–C_6 intermediates were quantified which demonstrate the effect of fuel molecular structure on pyrolysis. Numerical simulations were conducted using a detailed kinetic model from NUIG, and the differences in the pyrolysis chemistry of the isomers, and the formation of benzene is discussed.

2. Experiments

Experiments were performed using the NUIG single pulse shock tube (SPST), Fig. 1. The facility is described in detail in the Supplementary material (SM). 2M2B ($\geq$ 95%) was obtained from Sigma Aldrich. Trans-2-pentene (t-2-C_5H_{10}, $\geq$ 99%) was obtained from Fisher Scientific. 2M1B ($\geq$ 98%) and 3M1B ($\geq$ 95%) were obtained from TCI UK. Pureshield argon (Ar) supplied by BOC Ireland was used as the bath gas. 99.99% pure krypton (Kr) obtained from Sigma Aldrich was used as an internal standard. 99.9% pure helium supplied by BOC Ireland was used as the driver gas for all experiments. For all experiments, mixtures containing the 2% fuel, 0.5% Kr and 97.5% Ar were prepared based on partial pressures in a 40 L mixing vessel. KJLC capacitance manometers were used to monitor pressure levels.

The uncertainties in reflected temperatures are calculated based on the uncertainties in shock velocities and are approximately ±2% based on calculations suggested by Petersen et al. [16]. Uncertainties in calibrated species concentration are approximately ±10% and in estimated species concentrations, calculated using effective carbon number method [17], are approximately ±20% respectively. The uncertainty in reactant mole fractions is ±0.02%. The uncertainty in the residence time is ±2%. The 2σ variation in the calculated reflected pressures is approximately 8%. The MS system is used to identify and quantify Kr and an FID is used for all other organic species. The sample is introduced into a GS-Gaspro column through a split/split-less inlet which is maintained at 200 °C. Helium is used as the carrier gas and a constant flow rate of 0.9 ml min^{-1} is maintained through the column for all the experiments. The temperature programming of the GC was optimized for every fuel and the system was calibrated using a 23 gas GC standard obtained from BOC Ireland.

3. Kinetic modeling

Simulations were performed using Chemkin-Pro [18] assuming a closed homogeneous batch reactor at constant volume. We used the residence time approach for all our simulations in the range 3–4 ms, with details provided as SM [19]. The mechanism used to simulate the data is provided as SM.

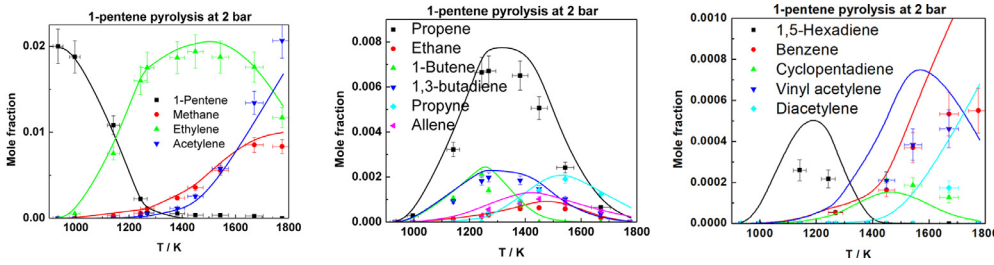

Fig. 2. Species profiles for 1-pentene pyrolysis. Solid lines: model simulations.

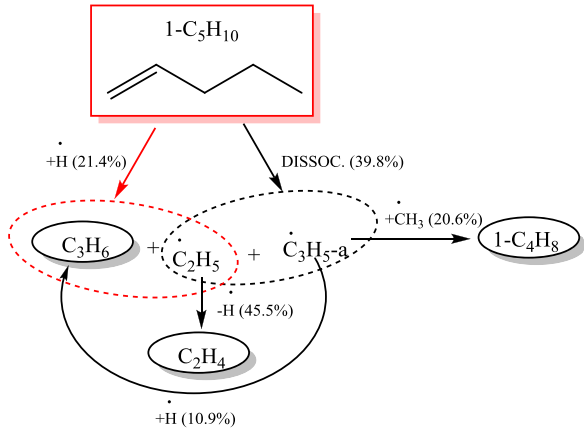

Fig. 3. RFD for 1-pentene pyrolysis at ~50% fuel consumption, 2.13 bar, 1243 K.

Reaction rates for Ḣ-atom abstraction by methyl ($\dot{C}H_3$) radicals from the fuel were obtained using rate rule analogy as shown by Cai et al. [20]. Rates for Ḣ-atom abstraction from primary, secondary and tertiary allylic sites were obtained from a theoretical study by Wang et al. [21].

3.1. Computational methods

The methods are similar to the ones in our previous studies of 1- and 2-pentene + Ḣ [22] and 1,3-pentadiene + Ḣ [23] and were adopted to calculate all electronic structure calculations for the 2M1B, 2M2B and 3M1B + Ḣ potential energy surfaces (PES), which is a current work-in-progress. Geometries of each minimum and transition state were optimized at the ωB97XD/aug-cc-pVTZ level of theory. Single point energies for minima and transition states were calculated at the CCSD(T)/cc-pVXZ and MP2/cc-pVXZ level, where $X = D$, T and Q levels of theory, which were then extrapolated to the complete basis set limit using Eq. (1) [2]:

$$E_{\mathrm{CCSD(T)/CBS}} = E_{\mathrm{CCSD(T)/cc-pVTZ}} + \left(E_{\mathrm{CCSD(T)/cc-pVTZ}} - E_{\mathrm{CCSD(T)/cc-pVDZ}}\right) \times \left(3^4/4^4 - 3^4\right) + E_{\mathrm{MP2/cc-PVQZ}} + \left(E_{\mathrm{MP2/cc-pVQZ}} - E_{\mathrm{MP2/cc-pVTZ}}\right) \times \left(4^4/5^4 - 4^4\right) - E_{\mathrm{MP2/cc-pVTZ}} - \left(E_{\mathrm{MP2/cc-pVTZ}} - E_{\mathrm{MP2/cc-pVDZ}}\right)\left(3^4/4^4 - 3^4\right). \quad (1)$$

High-pressure limiting and pressure dependent rate constants were calculated using RRKM theory with Master Equation (ME) analysis using the Master Equation System Solver, MESS, [24] which are available in the mechanism file provided as SM.

Thermochemical values for the C_5 species were calculated as a function of temperature (298–2000 K), with enthalpies of formation determined using a series of isodesmic reactions as described in our previous work [22]. Temperature-dependent enthalpies, entropies and heat capacities were then calculated using traditional statistical thermodynamics methods as implemented in MESSPF [24], with NASA polynomials fitted using PAC99 [25], which are provided as SM.

4. Results and discussion

In this section, we first present comparisons of the experimental and simulated mole fractions of the fuel and intermediates for the five pentene iso-

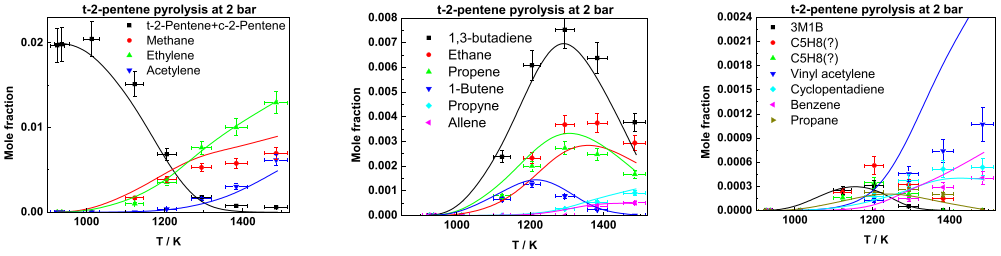

Fig. 4. Species profiles for t-2-pentene pyrolysis. Solid lines: model simulations.

mers. Thereafter, by comparing the mole fractions of the intermediates produced during the pyrolysis of the five isomers, we analyze the effect of molecular structure on the pyrolysis chemistry.

4.1. 1-Pentene

Experimental data for 1-pentene (1-C_5H_{10}) is taken from our article on the pyrolysis of 1-alkenes [26]. The current mechanism's predictions are shown in Fig. 2. A reaction flux diagram (RFD) for 1-pentene pyrolysis at 1243 K is provided in Fig. 3.

Based on kinetic simulations, 1-pentene decomposes to form either allyl and an ethyl radical or undergoes a retro-ene reaction to produce ethylene and propene. Bimolecular reactions of 1-pentene with $\dot{H}$ atoms can produce propene (C_3H_6) and ethyl radicals ($\dot{C}_2H_5$) or ethylene (C_2H_4) and *n*-propyl (*n*-$\dot{C}_3H_7$) radicals. H-atom abstraction from 1-pentene produces 1-penten-3-yl ($\dot{C}_5H_9$1-3) radicals which dissociate into 1,3-butadiene (1,3-C_4H_6) and methyl radicals. Allyl radicals ($\dot{C}_3H_5$-a) decompose to form allene (C_3H_4-a) and $\dot{H}$ atoms and/or their self-disproportionation reaction produces allene and propene. They can also undergo radical-recombination reaction with $\dot{C}H_3$ radicals to form 1-butene (1-C_4H_8). The self-recombination of methyl radicals and the allyl + ethyl disproportionation reaction are the main sources of ethane (C_2H_6). Propyne (C_3H_4-p) is produced via the isomerization of allene. Methane (CH_4) is produced via H-atom abstraction by $\dot{C}H_3$ radicals from the fuel and other stable intermediate species. Acetylene (C_2H_2) is produced from the dissociation of vinyl radicals and the bimolecular reactions of allene and propyne with $\dot{H}$ atoms.

4.2. trans-2-Pentene

Pyrolysis experiments of t-2-C_5H_{10} were carried out at 2 bar in the range of 900–1500 K. The major products are methane, ethane, ethylene, acetylene, propene, 1-butene, 1,3-butadiene, allene and propyne. The species profiles are illustrated in Fig. 4. We found two C_5H_8 species but could not distinguish them as the mass spectra of pentadienes are similar. However, from studies by Manion and Awan [12], one species can be assigned 1,3-pentadiene and the other could be cyclopentene. We also observe the formation of cis-2-pentene (c-2-C_5H_{10}). We believe this could be similar to the cis/trans isomerization of 2-butene as discussed by Lifshitz et al. [27]. An earlier ignition delay time study on 2-butenes [28] had shown that the reactivities were similar for the cis and trans isomers and therefore, the current mechanism includes one species to represent both.

A reaction pathway analysis diagram for t-2-pentene pyrolysis is provided in Fig. 5. Trans-2-pentene can decompose into $\dot{C}H_3$ and 1-buten-3-yl ($\dot{C}_4H_7$1–3) radicals, $\dot{C}_4H_7$1–3 subsequently produces 1,3-butadiene via H-atom elimination. The fuel and intermediates can undergo $\dot{H}$-atom abstraction by $\dot{C}H_3$ radicals to form methane. The reaction of 2-pentene with $\dot{H}$ atoms produces propene and ethyl radicals. Ethyl radi-

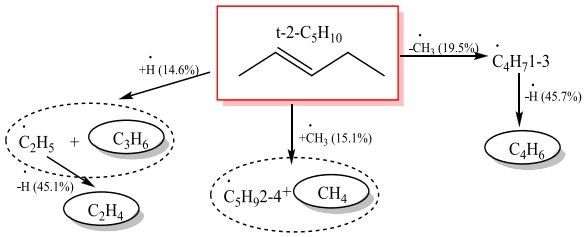

Fig. 5. RFD for t-2-pentene pyrolysis at ~50% fuel consumption, 2.01 bar, 1205.4 K.

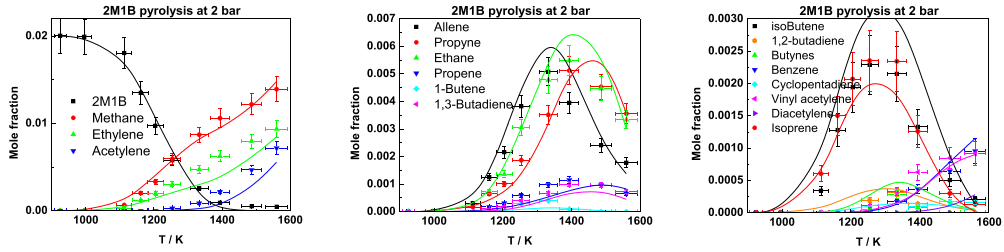

Fig. 6. Species profiles for 2M1B pyrolysis. Solid lines: model simulations.

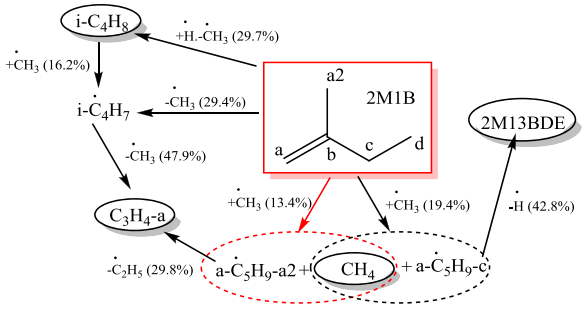

Fig. 7. RFD for 2M1B pyrolysis at ~50% fuel consumption, 2.01 bar, 1254.2 K.

cals undergo β-scission to produce ethylene and $\dot{H}$ atoms. Ethane is produced via $\dot{C}H_3$ radical self-recombination. Acetylene formation channels are similar to those for 1-pentene as discussed earlier.

4.3. 2-methyl-1-butene

2-methyl-1-butene pyrolysis study was carried out at 2 bar in the range of 900–1600 K. The major products are methane, ethane, ethylene, acetylene, propene, allene, propyne, isobutene (i-C_4H_8), 1,3-butadiene and isoprene (2M13BDE). Species profiles are shown in Fig. 6.

2M1B can dissociate into 2-methyl-allyl (i-$\dot{C}_4H_7$) and methyl radicals or can react with $\dot{H}$ atoms to form isobutene. It can also undergo H-atom abstraction by $\dot{C}H_3$ radicals or $\dot{H}$ atoms from the primary and secondary allylic site to form 2-methyl-1-butenyl (a$\dot{C}_5H_9$-a2) and 2-methyl-1-buten-3-yl (a$\dot{C}_5H_9$-c) radicals, respectively. a$\dot{C}_5H_9$-c radicals dissociate to form isoprene and a$\dot{C}_5H_9$-a2 radicals dissociate to form allene and ethyl radicals. Also, 2-methyl-allyl radicals decompose to form allene and $\dot{C}H_3$ radicals. a$\dot{C}_5H_9$-a2 radicals can isomerize to form 2-methyl-1-buten-4-yl (a$\dot{C}_5H_9$-d) radicals. These dissociate to form ethylene and propen-2-yl ($\dot{C}_3H_5$-t) radicals which in turn dissociate to form propyne and $\dot{H}$ atoms. Propyne is also formed by isomerization of allene. Methane, ethane, ethylene and acetylene formation reactions are similar to those for the linear pentenes. The RFD for 2M1B pyrolysis is shown in Fig. 7.

4.4. 2-methyl-2-butene

A pyrolysis study was carried out at 2 bar and in the temperature range of 900–1750 K and the major species are identical to 2M1B pyrolysis, Fig. 8 2M2B and isoprene co-elute in the GC capillary column used in this study and could not be separated, so for comparison we show the sum of the two molecules in both experiments and simulations.

2M2B (b-C_5H_{10}) can undergo H-atom abstraction by $\dot{H}$ atoms and $\dot{C}H_3$ radicals from three primary allylic sites to form isopentenyl radicals. These radicals form isoprene via H-atom elimination. 2M2B can also react with $\dot{H}$ atoms to produce isobutene and methyl radicals. Isobutene dissociates to methyl-allyl (i$\dot{C}_4H_7$) radicals which further dissociate to form allene and $\dot{C}H_3$ radicals. The current mechanism under-predicts the formation of 1,3-C_4H_6 by a factor of two. Propene is formed from isopentenyl radicals and isobutene. Ethane, ethylene, methane and acetylene formation pathways for 2M1B and 2M2B are the same. An RFD for 2M2B pyrolysis is illustrated in Fig. 9.

4.5. 3-methyl-1-butene

3M1B has a tertiary-allylic hydrogen and it assisted to examine the rate law for such H-atom abstractions. 3M1B pyrolysis study was carried out

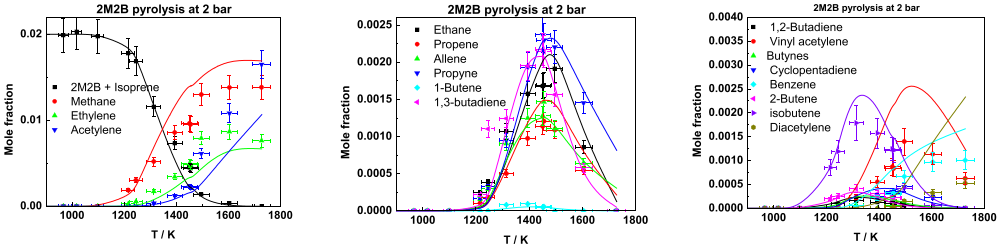

Fig. 8. Species profile for 2M2B pyrolysis. Solid lines: model simulations.

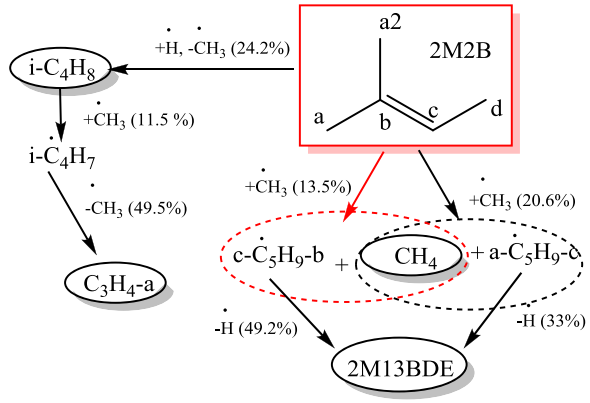

Fig. 9. RFD for 2M2B pyrolysis at ~50% fuel consumption, 2.13 bar, 1451.2 K.

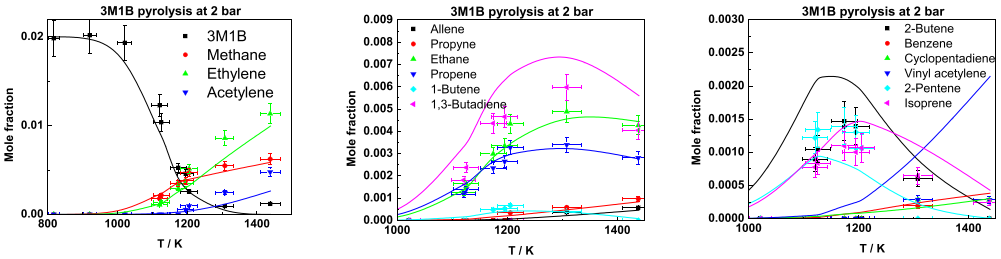

Fig. 10. Species profile for 3M1B pyrolysis. Solid lines: model simulations.

at 2 bar and 800–1450 K. Methane, ethylene, acetylene, propene, 2-butene, 1,3-butadiene, 2-pentene and isoprene are major products. Species profiles with respect to temperature are illustrated in Fig. 10.

3M1B (c-C_5H_{10}) can either decompose to 1-buten-3-yl ($\dot{C}_4H_7$1-3) radicals or react with $\dot{H}$ atoms to form 2-butene (2-C_4H_8). 3M1B can also undergo H-atom abstraction by $\dot{H}$ atoms or $\dot{C}H_3$ radicals from the tertiary allylic site to form isopentenyl radicals which dissociate to isoprene. $\dot{C}_4H_7$1-3 radicals dissociate to 1,3-butadiene via β-scission. 2-butene reacts with $\dot{H}$ atoms to form propene and methyl radicals. Ethylene is formed from c-C_5H_{10}+$\dot{H}$, 1,3-C_4H_6+$\dot{H}$ and ethyl radical decomposition reactions. Ethane, methane and acetylene formation reactions are similar to all of the other pentenes. An RFD at 1205 K is provided as Fig. 11.

5. Discussion

5.1. Fuel reactivities and ethylene formation

From our experimental measurements, we were able to determine that the predicted reactivities of all of the pentenes are sufficiently accurate, Fig. 12. The reactivities appear to decrease with increasing number of allylic hydrogen atoms. 3M1B, with only tertiary allylic hydrogen has the highest reactivity and 2M2B with nine primary allylic hy-

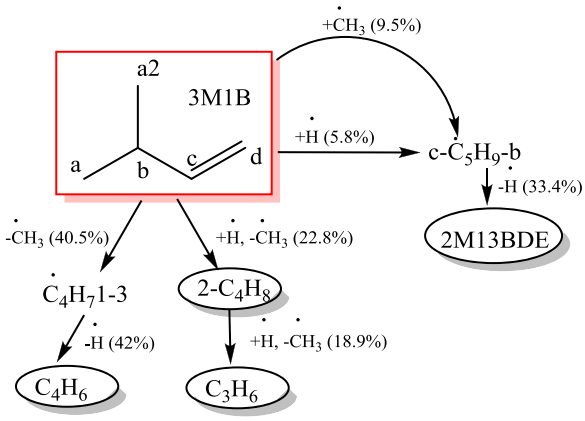

Fig. 11. RFD for 3M1B pyrolysis at ~50% fuel consumption, 2.01 bar, 1205 K.

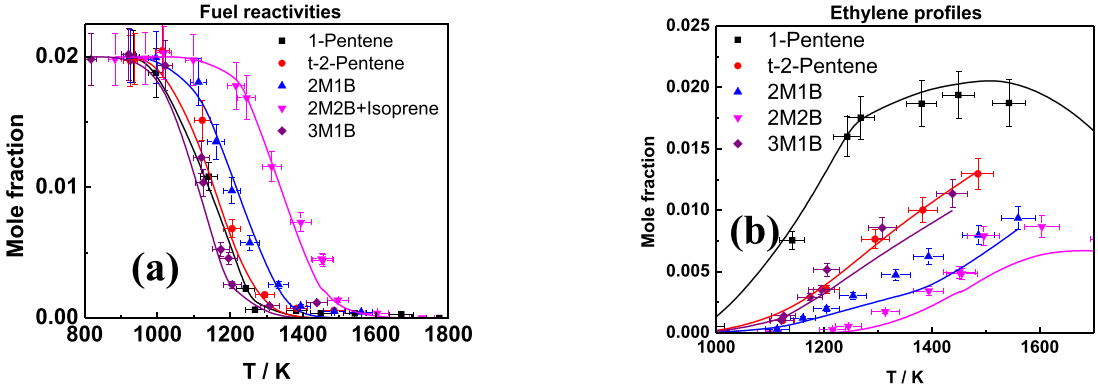

Fig. 12. (a) Fuel reactivities for pentenes and (b) ethylene formation. Solid lines: model simulations.

drogen atoms has the lowest reactivity, while linear pentenes with secondary allylic hydrogen atoms show intermediate reactivity.

Ethylene is one of the initial stable products, with its concentrations and shape being significantly higher and different for 1-pentene corroborating the presence of the retro-ene reaction. For the other isomers, 3M1B and t-2-pentene show similar concentrations due to their initial unimolecular decomposition reactions producing $\dot{C}H_3 + \dot{C}_4H_71\text{–}3 \rightarrow 1,3\text{-}C_4H_6 + \dot{H} \rightarrow C_2H_4 + \dot{C}_2H_3$ and $\dot{C}H_3 + \dot{C}H_3 \rightarrow C_2H_6 + R \rightarrow RH + \dot{C}_2H_5 \rightarrow C_2H_4 + \dot{H}$.

5.2. Formation of benzene and aromatic precursors

The reactions illustrated in Fig. 13 show some of the important reactions of the C_3–C_5 intermediates forming benzene. We compared the concentrations of these intermediates and conducted flux analyses to illustrate how the important pathways for benzene changes with isomer molecular structure.

Trans-2-pentene and 3M1B produce higher concentrations of 1,3-butadiene due to their initial unimolecular decomposition into 1-buten-3-yl radical, Fig. 14(a). At > 90% fuel consumption, the amount of cyclopentadiene produced is higher for 2M2B and t-2-pentene compared to the other isomers, Fig. 14(b). This appears to show the significance of

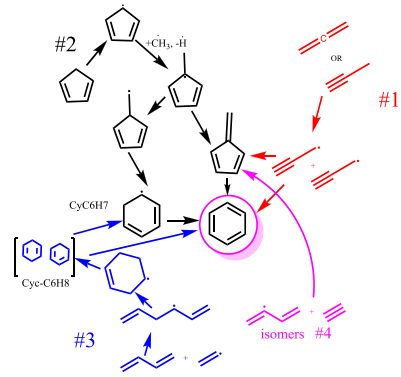

Fig. 13. Benzene formation pathways.

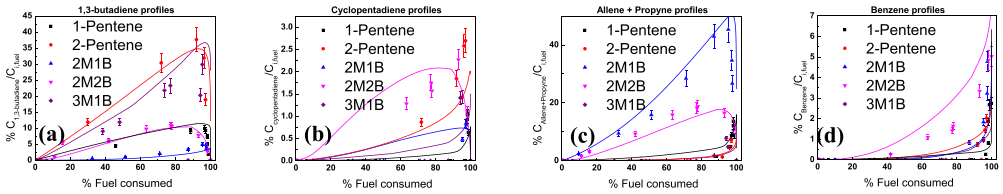

Fig. 14. Experiment results for (a) 1,3-butadiene concentration; (b) Cyclopentadiene concentration; (c) Allene and propyne total concentration and (d) Benzene concentration. Fuel consumed is calculated as (initial fuel concentration – final fuel concentration)/initial fuel concentration at a given temperature. This aids in offsetting the effect of fuel reactivity.

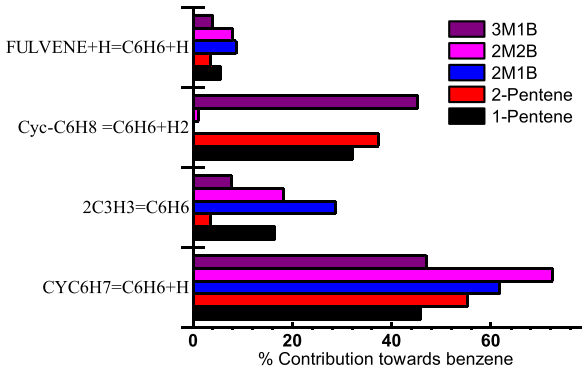

Fig. 15. Relative ROP of Benzene at 1400 K and 2 bar.

the location of the double bond on the formation of cyclopentadiene.

The concentrations of allene and propyne are higher in the pyrolysis of 2M1B, Fig. 6, owing to the unimolecular decomposition of the fuel to 2-methyl-allyl radicals and abstraction from the primary allylic site, both of which undergo β-scission to produce allene, Fig. 14(c). 2M2B also produces lower amounts of allene and propyne compared to 2M1B due to the absence of a direct route to the formation of 2-methyl-allyl radical, Fig. 8. An efficient way to allene and propyne is through abstractions from isobutene, produced from 2M2B+$\dot{H}$=isobutene+$\dot{C}H_3$, to produce 2-methyl-allyl radicals and subsequent decomposition of these to allene+$\dot{C}H_3$. The absence of direct pathway to the formation of 2-methyl-allyl radicals explains the difference in concentrations of the C_3H_4 isomers produced during the pyrolysis of 2M1B and 2M2B. Interestingly, the concentrations of benzene presented in Fig. 14(d) shows that 2M2B produces more benzene than all of the other isomers. Also, the predictions from the mechanism are satisfactory.

To gain insights into the effect of molecular structure on pyrolysis chemistry, we conducted an integrated reaction path analysis of the different pathways to identify differences in the chemistry producing benzene, Fig. 15. It can be seen that propargyl recombination is important for benzene formation. Moreover, the $\dot{C}_5H_5$+$\dot{C}H_3$ reaction pathway is crucial for benzene formation irrespective of the geometry of the molecule. Furthermore, vinyl addition to 1,3-butadiene seems important for linear pentenes and for 3M1B. Interestingly, the HACA mechanism is relatively less important than the propargyl pathway [29] as the bimolecular reaction of 1,3-butadiene with $\dot{H}$ atoms to produce ethylene and vinyl radicals dominates over H-atom abstraction by $\dot{H}$ atoms [30].

6. Conclusions

A SPST pyrolysis study was carried out on t-2-pentene, 2M1B, 2M2B and 3M1B at 2 bar. Species were identified using GC–MS and were quantified using an FID. High-pressure limiting and pressure dependent rate constants for 2M1B, 2M2B and 3M1B + $\dot{H}$ were calculated using RRKM theory with Master Equation (ME) analysis. A mechanism was formulated based on rate rules and the theoretical calculations. Comparisons between experimental and simulated results show that the predictions for all of the major species are satisfactory. Furthermore, reactivities of the fuels studied clearly show the influence of molecular geometry on unimolecular dissociation and H-atom abstractions from different allylic sites. Also, the molecular geometry impacts the benzene formation pathways and this study shows that 2M2B produces more benzene than other pentenes. In addition, the HACA mech-

anism has a relatively lower prominence for benzene formation compared to other pathways.

Declaration of Competing Interest

None.

Acknowledgments

The authors would like to acknowledge Science Foundation Ireland for funding via project numbers 15/IA/3177 and 16/SP/3829. The work at LLNL was performed under the auspices of the U.S. Department of Energy (DOE), Contract DE-AC52-07NA27344, and was supported by the U.S. Department of Energy, Vehicle Technologies Office, program managers, Mike Weismiller and Gurpreet Singh.

Supplementary materials

Supplementary material associated with this article can be found, in the online version, at doi:10.1016/j.proci.2020.06.069.

References

[1] M. Mehl, T. Faravelli, F. Giavazzi, et al., *Energy Fuels* 20 (2006) 2391–2398, doi:10.1021/ef060339s.
[2] J.A. Miller, S.J. Klippenstein, *J. Phys. Chem. A* 107 (2003) 7783–7799, doi:10.1021/jp030375h.
[3] H. Wang, M. Frenklach, *Combust. Flame* 110 (1997) 173–221, doi:10.1016/S0010-2180(97)00068-0.
[4] S. Sharma, W.H. Green, *J. Phys. Chem. A* 113 (2009) 8871–8882, doi:10.1021/jp900679t.
[5] C. Cavallotti, D. Polino, A. Frassoldati, E. Ranzi, *J. Phys. Chem. A* 116 (2012) 3313–3324, doi:10.1021/jp212151p.
[6] L. Ruwe, L. Cai, K. Moshammer, N. Hansen, H. Pitsch, K. Kohse–Höinghaus, *Combust. Flame* (2019) 411–423, doi:10.1016/j.combustflame.2019.05.013.
[7] G. González Alatorre, H. Böhm, B. Atakan, K. Kohse-Höinghaus, *Z. Phys. Chem.* 215 (2001) 981–995, doi:10.1524/zpch.2001.215.8.981.
[8] R. Minetti, A. Roubaud, E. Therssen, M. Ribaucour, L. Sochet, *Combust. Flame* 118 (1999) 213–220, doi:10.1016/S0010-2180(98)00151-5.
[9] Y. Cheng, E. Hu, X. Lu, et al., *Proc. Combust. Inst.* 36 (2017) 1279–1286, doi:10.1016/J.PROCI.2016.08.026.
[10] S. Touchard, F. Buda, G. Dayma, P.A. Glaude, R. Fournet, F. Battin-Leclerc, *Int. J. Chem. Kinet.* 37 (2005) 451–463, doi:10.1002/kin.20096.
[11] W. Tsang, *Int. J. Chem. Kinet.* 10 (1978) 599–617, doi:10.1002/kin.550100607.
[12] J.A. Manion, I.A. Awan, *Proc. Combust. Inst.* 34 (2013) 537–545, doi:10.1016/j.proci.2012.05.078.
[13] C.K. Westbrook, W.J. Pitz, et al., *J. Phys. Chem. A* 119 (2015) 7462–7480, doi:10.1021/acs.jpca.5b00687.
[14] L. Ruwe, K. Moshammer, N. Hansen, K. Kohse-Höinghaus, *Combust. Flame* 175 (2017) 34–46, doi:10.1016/J.COMBUSTFLAME.2016.06.032.
[15] L. Ruwe, K. Moshammer, N. Hansen, K. Kohse-Höinghaus, *Phys. Chem. Chem. Phys.* 20 (2018) 10780–10795, doi:10.1039/C7CP07743B.
[16] E.L. Petersen, M.J.A. Rickard, M.W. Crofton, E.D. Abbey, M.J. Traum, D.M. Kalitan, *Meas. Sci. Technol.* 16 (2005) 1716–1729, doi:10.1088/0957-0233/16/9/003.
[17] J.T. Scanlon, D.E. Willis, *J. Chromatogr. Sci.* 23 (1985) 333–340, doi:10.1093/chromsci/23.8.333.
[18] R. CHEMKIN-PRO, 15112, Reaction Design, Inc., San Diego, CA. (2011).
[19] X. Han, J.M. Mehta, K. Brezinsky, *Combust. Flame* 209 (2019) 1–12, doi:10.1016/j.combustflame.2019.07.022.
[20] L. Cai, H. Pitsch, S.Y. Mohamed, *Combust. Flame* 173 (2016) 468–482, doi:10.1016/j.combustflame.2016.04.022.
[21] K. Wang, S.M. Villano, A.M. Dean, *Phys. Chem. Chem. Phys.* 17 (2015) 6255–6273, doi:10.1039/c4cp05308g.
[22] J. Power, K.P. Somers, C.-.W. Zhou, S. Peukert, H.J. Curran, *J. Phys. Chem. A* (2019), doi:10.1021/acs.jpca.9b06378.
[23] Y. Sun, C.-.W. Zhou, K.P. Somers, H.J. Curran, *J. Phys. Chem. A* (2019), doi:10.1021/acs.jpca.9b06628.
[24] Y. Georgievskii, J.A. Miller, M.P. Burke, S.J. Klippenstein, *J. Phys. Chem. A* 117 (2013) 12146–12154, doi:10.1021/jp4060704.
[25] B.J. McBride, S. Gordon, Computer Program for Calculating and Fitting Thermodynamic Functions, (1992).
[26] S.S. Nagaraja, J. Liang, S. Dong, S. Panigrahy, A.B. Sahu, G. Kukkadapu, W.J. Pitz, H.J. Curran, *Combust. Flame* 219 (2020) 456–466.
[27] A. Lifshitz, S.H. Bauer, E.L. Resler, *J. Chem. Phys.* 38 (1963) 2056–2063, doi:10.1063/1.1733933.
[28] Y. Li, C.W. Zhou, K.P. Somers, K. Zhang, H.J. Curran, *Proc. Combust. Inst.* 36 (2017) 403–411, doi:10.1016/j.proci.2016.05.052.
[29] J.A. Miller, C.F. Melius, *Combust. Flame* 91 (1992) 21–39, doi:10.1016/0010-2180(92)90124-8.
[30] Y. Li, S.J. Klippenstein, C.-.W. Zhou, H.J. Curran, *J. Phys. Chem. A* 121 (2017) 7433–7445, doi:10.1021/acs.jpca.7b05996.